Water-soluble vitamins for controlling starch digestion: Conformational scrambling and inhibition mechanism of human pancreatic α-amylase by ascorbic acid and folic acid

Pallab Kumar BORAH [a, b], Anwesha SARKAR [b], Raj Kumar DUARY [a]*

[a]Department of Food Engineering and Technology, School of Engineering, Tezpur University, 784 028, India

[b]Food Colloids and Processing Group, School of Food Science and Nutrition, University of Leeds, LS2 9JT, United Kingdom

Corresponding Author

Dr. Raj Kumar Duary, E-mail address: duary@tezu.ernet.in, rkduary@gmail.com; Phone No.: +91-3712-275709; Fax: +91-03712-267005.

E-mail addresses of all co-authors: pallab@tezu.ernet.in (Pallab Kumar Borah), A.sarkar@leeds.ac.uk (Anwesha Sarkar), duary@tezu.ernet.in, rkduary@gmail.com (Raj Kumar Duary).

Abstract

The inhibition of human pancreatic α-amylase (HPA) enzyme activity can offers facile routes to ameliorate postprandial hyperglycemia in diabetes via control of starch digestion. The present study utilizes complementary experimental (starch digestion kinetics, fluorescence quenching, Förster resonance energy transfer, and X-ray diffraction) and computational (molecular docking and dynamics simulation) methods to evaluate for the first time the HPA inhibitory activity of eight water-soluble vitamins. In particular, ascorbic acid inhibited HPA activity via non-competitive antagonism from two allosteric sites, by channeling the inhibition towards the active site cavity via the triose-phosphate isomerase (TIM) barrel. Whereas folic acid inhibited HPA activity by binding competitively at the active site cavity and decreasing the disorder in the neighboring loop 3 and 7, the latter are important mobile loops in HPA for starch digestion. The infusion of such biocompatible and nutritional water-soluble vitamins alongside starch may enable avenues in diabetes management.

Abbreviations

HPA, human pancreatic α-amylase; FRET, Förster resonance energy transfer; RMSD, root mean square deviation; RMSF, root mean square fluctuation; PC, principal component; Cα, alpha carbon in an organic molecules; cf., compare; Asp, Aspartic acid; Glu, Glutamic acid; Trp, Tryptophan; Tyr, Tyrosine; Lys, Lysine; Arg, Arginine; Thr, Threonine; Ala, Alanine; Asn, Asparagine; Pro, Proline; Gly, Glycine; Phe, Phenylalanine; His, Histidine.

Keywords

Pancreatic α-amylase; starch digestion; inhibition mechanism; water-soluble vitamins; ascorbic acid; folic acid.

Chemical compounds studied in this article

Ascorbic acid (PubChem CID: 54670067); Folic acid (PubChem CID: 6037)

1. Introduction

Water-soluble vitamins are nutritional components in food that are greatly required by individuals for proper health and functioning. Therefore quite naturally, their deficiency is known to affect the health of an individual negatively and cause numerous diseases, such as scurvy in the case of ascorbic acid deficiency (Spoelstra-de Man, Elbers, & Oudemans-Van Straaten, 2018), and cancers, neural tube defects, megaloblastic anemia, and psychiatric disorders in the case of folic acid deficiency (Shi, Wang, Zhang, Liu, & Fei, 2017).

In addition to that, researchers have also observed that some of these water-soluble vitamins have the ability to inhibit α-amylase activity (Abell, Ratcliffe, & Gerrard, 1998; Kim, Kang, Lee, Chang, Lee, Apostolidis, et al., 2018; Shi, Wang, Zhang, Liu, & Fei, 2017). The latter is an endoglycosidase, responsible for the cleavage of α-1, 4-linked glucose subunits of starch to produce maltose, maltotriose, and limit dextrins (Butterworth, Warren, & Ellis, 2011). The enzyme α-amylase lies at the top of the chain of enzymes that are collectively responsible for breaking down starch into glucose monomers. Although, starch digestion into glucose is critical for energy and survival, in the past few decades, excessive ingestion and digestion of dietary starches have been related to spikes in postprandial blood glucose levels leading to difficulties in the management of hyperglycemia in diabetic individuals. As such, mitigating the activity of α-amylase has been directly correlated with the management of food-linked hyperglycemia.

Among such water-soluble vitamins, ascorbic acid has been reported to be a potent inhibitor of malt, bacterial, fungal, and porcine pancreatic and salivary α-amylases, decreasing

enzyme activity by 100% (Abell, Ratcliffe, & Gerrard, 1998). Authors reported the structure-activity information of ascorbic acid for α-amylase inhibition, and proposed that the enediol moiety of the vitamin is essential for the inhibition mechanism. Also, ascorbic acid supplementation resulted in improved postprandial glucose responses in people with type-II diabetes (Mason, Rasmussen, & Wadley, 2018). The group additionally reported that such treatments were well tolerated by the individuals, without any adverse side-effects. Recently, folic acid has also been reported to be an inhibitor of porcine pancreatic α-amylase. Here, 0.0004 mol L^{-1} folic acid was reported to reduce the relative activity of porcine pancreatic α-amylase by 70% (Shi, Wang, Zhang, Liu, & Fei, 2017). Using computational molecular modeling studies, the authors additionally reported that the inhibition mechanism was directed via folic acid binding to the substrate-binding pocket (active site) of the porcine pancreatic α-amylase. Additionally, pyridoxine has also been reported to be a weak inhibitor of porcine pancreatic α-amylase, with IC_{50} values of 23.18 mg mL^{-1} (Kim, Kang, Lee, Chang, Lee, Apostolidis, et al., 2018). The reaction mechanism and molecular mode of inhibition is yet to be explored.

The scenario presents us with an interesting companionship for formulation design of food structure (Borah, Rappolt, Duary, & Sarkar, 2019) where biocompatible and nutritional water-soluble vitamins can be infused with starch for controlling meal-associated glucose spikes in blood. However, the mechanism by which these water-soluble vitamins inhibit HPA has remained partly elusive. Existing literature on the topic has been explored using porcine pancreatic α-amylase. It remains unclear as to how these findings from porcine systems can be applied to the human pancreatic α-amylase (HPA), considering a significant difference in amino acid sequence between these variants (Brayer, Luo, & Withers, 1995).

Noteworthy, imminent advances in the utilization of water-soluble vitamins as potential inhibitors of HPA in the human diet can only be achieved with a better

understanding of functional and structural mechanisms behind such inhibition. The current study for the first time explores the inhibition of HPA by eight water-soluble vitamins. We systematically characterize the inhibition mechanism and conformational scrambling induced by ascorbic acid and folic acid on HPA leading up to the inhibition of the latter, using complementary experimental (starch digestion kinetics), spectral (X-ray diffraction, fluorescence quenching and Förster resonance energy transfer) and computational (molecular docking, dynamic simulations) methods. The computational studies allow us to obtain atomistic-scale details about the behavior of inhibitors at its binding site(s), further insights into molecular events, and assist in comprehending the conformational reorganization and dynamics in the enzyme structure. Such approaches have been widely exploited by researchers to probe into the interaction mechanism of α-amylases with various inhibitors such as myricetin, ethyl caffeate, pentagalloyl-glucose, etc (Kato-Schwartz, Bracht, Gonçalves, Soares, Vieira, Brugnari, et al., 2018; Williams, Li, Withers, & Brayer, 2012). With the current clinically existing inhibitors such as acarbose and miglitol showing lower compliance in individuals (Williams, Li, Withers, & Brayer, 2012), the present study should constitute a solid-framework for the future development of low glycemic food structures involving starch. Amylopectin corn starch was used in this study as the substrate model because amylopectin forms the major component of widely consumed cereal starches.

2. Materials and methods

2.1. Materials

Amylopectin corn starch, folic acid, riboflavin, acarbose, 3, 5-dinitrosalicylic acid (DNSA), dimethyl sulfoxide (DMSO) and human pancreatic α-amylase (≥100 U mg^{-1}) were purchased from Sigma-Aldrich, India. Ascorbic acid, thiamine, pantothenic acid, pyridoxine, biotin, and

niacin were purchased from Sisco Research Laboratories, India. A highly quenched BODIPY FL starch derivative (DQ starch, part of an EnzCheck® Ultra α-amylase assay kit) was purchased from Life Technologies Co., USA. All starch solutions were prepared in phosphate saline (PBS) buffer (0.01 M, NaCl 0.1 M, and pH 7.4 at 25 ° C) and heated (to simulate cooking or processing) at 90 °C for 20 min. All the water-soluble vitamin solutions were prepared in 20% DMSO in PBS buffer. For all fluorescence measurements, the HPA stock solution was filtered through 0.45 µm filter in order to avoid artefacts caused by unintentional incorporation of dust or presence of any aggregated proteins. Milli-Q water (Millipore Corp., Bedford, MA, USA) was used throughout the experiments (18.2 MΩcm ionic purity at 25 °C).

2.2. Screening for HPA inhibitory activity by water-soluble vitamins

The reaction velocity (v) for starch digestion (10 mg mL^{-1}) by HPA (14.8 U mL^{-1}) in presence of the water-soluble vitamins (10 mg mL^{-1}) was measured as described previously (Sun, Chen, Meng, Yang, Yuan, & Guo, 2016). Acarbose was used as a reference inhibitor at 10 mg mL^{-1}. The release of maltose equivalent was monitored using a high-throughput 3, 5-dinitrosalicylic acid (DNSA) method at 575 nm (Gonçalves, Rodriguez-Jasso, Gomes, Teixeira, & Belo, 2010; Miller, 1959). The v was determined at 37 °C from the slope of mM maltose min^{-1}.

2.3. Estimation of HPA inhibition

The method used for the estimation of HPA inhibition was adapted from a previous report (Yilmazer-Musa, Griffith, Michels, Schneider, & Frei, 2012). Exactly 0.19 U mL^{-1} of HPA solution was used for the experiment. Measurements were taken six times at an interval of 5 min at λ_{ex} = 460 nm and λ_{em} = 520 nm, and expressed as the slope of linear correlation ($\Delta_{fluorescence}$ min^{-1}). The percentage of inhibition (I) was estimated as,

$$I = \left(1 - \left(\frac{v}{v_o}\right)\right) 100 \qquad \text{Eq. (1)}$$

where v was the initial reaction velocity in the presence of the water-soluble vitamins, and v_o was the reaction velocity in the absence of the water-soluble vitamins.

The half maximal inhibitory concentration (IC_{50}) values were estimated using a non-linear sigmoidal fitting function in Origin Pro 8.5.0 (OriginLab Corporation, Northhampton, USA).

2.4. Investigating the detailed kinetics

The water-soluble vitamin solutions at various concentrations (i) and HPA solution (14.8 U mL^{-1}) were pre-incubated at 4 °C for 20 min, followed by the addition of appropriate dilutions of the starch solution. The values of v were determined at 37°C from the slope of mM maltose min^{-1}.

At differing water-soluble vitamin (inhibitor) concentrations (i), the apparent Michaelis constant (K_m^{app}) and the apparent maximum reaction velocity (V_{max}^{app}) were estimated by nonlinear regression analysis using the Michaelis–Menten equation in GraphPad Prism Software version 7.0 (GraphPad software Inc., USA).

The kinetic parameters obtained from the nonlinear regression analysis were used for the following analysis. The linear Lineweaver Burk form of the modified Michaelis-Menten equation was plotted as,

$$\frac{1}{v} = \frac{K_m^{app}}{V_{max}^{app}} \cdot \frac{1}{s} + \frac{1}{V_{max}^{app}} \quad \text{Eq. (2)}$$

Eq. (2) described the linear relationship between 1/v versus 1/s at respective i, s was the concentration of starch.

The inhibitor dissociation constants, K_{ic} for the competitive inhibition was estimated as,

$$v = \frac{V_{max}^{app} s}{K_m^{app}\left(1+\frac{1}{K_{ic}}\right)+s} \quad \text{Eq. (3)}$$

The inhibitor dissociation constants, K_{ic} for competitive inhibition and K_{in} for non-competitive inhibition were estimated as,

$$v = \frac{V_{max}^{app} s}{K_m^{app}\left(1+\frac{1}{K_{ic}}\right)+s\left(1+\frac{1}{K_{in}}\right)} \quad \text{Eq. (4)}$$

Here, using a reciprocal of both the sides, 1/v versus i describes a Dixon plot. Using two independent starch concentrations, $K_{ic} = -i$ for both Eq. (3) and (4), the measure of the abscissa of intersection amidst multiple Dixon plots at independent starch concentrations was equal to the K_{ic}.

A value of K_{in} was derived by plotting s/v versus i at respective s. This was expressed as,

$$\frac{v}{s} = \frac{V_{max}^{app}}{K_m^{app}\left(1+\frac{1}{K_{ic}}\right)+s\left(1+\frac{1}{K_{in}}\right)} \quad \text{Eq. (5)}$$

Again, using a reciprocal of both the sides, s/v versus i describes an Eisenthal-Cornish-Bowden plot. As described above, $K_{in} = -i$ for Eq (5), the measure of the abscissa of intersection amidst multiple Eisenthal-Cornish-Bowden plots at independent starch concentrations should equal to the K_{in}.

2.5. X-ray diffraction (XRD)

The XRD spectra (angular range, 2θ = 5–27°) of the dry powder samples were obtained using a D8 Focus X-ray (Cu Kα radiation, λ = 0.154 nm) diffractometer (Bruker AXS, Germany) at 25 °C.

2.6. Fluorescence spectroscopy analysis

Water-soluble vitamin solutions were incubated (at 4 °C for 30 min) with 75 U mL^{-1} HPA solution. The final concentration of water-soluble vitamin in the mixture was 0.00025 – 0.008 mg mL^{-1}. The DMSO concentrations in the final mixture was > 0.1 %, and therefore should not affect the HPA activity. The intrinsic fluorescence spectra of HPA at different i concentrations were measured at two different temperatures (300 and 310 K) using λ_{ex} = 280 nm and λ_{em} = 300 - 450 nm, with slit widths at 10 nm.

Inner filter effect was minimized as per previous report (Gayen, Chatterjee, & Mukhopadhyay, 2008),

$$F_{corr} = F_{obs} \times e^{\frac{(A_{ex}+A_{em})}{2}} \quad \text{Eq. (6)}$$

where F_{corr} and F_{obs} describes the corrected and the observed fluorescence intensities, and, A_{ex} and A_{em} described the absorption within the systems at λ_{ex} and λ_{em}, respectively.

Collisional effect were probed by estimating the fluorescence spectra of free L-tryptophan (Trp) amino acid residues in the aforementioned conditions.

2.7. Molecular docking

The crystal structures of the human pancreatic α-amylase enzyme (PDB ID: 1HNY) was retrieved from the RCSB Protein Data Bank (http://www.rcsb.org/pdb). All crystallographic water molecules and a co-crystallized pyroglutamic acid ligand were removed, alongside the addition of polar hydrogens and Geisteiger charges to the protein model.

The 3-dimensional ligand structures of the ascorbic acid and folic acid molecules were retrieved from the PubChem database (https://pubchem.ncbi.nlm.nih.gov/). Energy minimization of the ligands were performed using the steepest descent algorithm employing

the universal force field (UFF) until convergence ($\Delta E = 1 \times 10^{-7}$ KJ mol^{-1}) in Avogardo 1.2.0 (http://avogadro.openmolecules.net). The resultant geometry were optimized using B3LYP hybrid density functional theory using the 6-31G** basis set in ORCA 4.0.1.2 (Neese, 2012). A co-crystallized maltopentaose ligand was extracted from the X-ray crystallographic structure of α-amylase from Bacillus subtilis (PDB ID: 1BAG), and used without structural optimization.

Molecular docking was performed in Autodock 4.2 (Morris, Huey, Lindstrom, Sanner, Belew, Goodsell, et al., 2009) employing 126 grid points (in a xyz coordinate system) with a spacing of 0.375 Å. The Lamarckian genetic algorithm was employed with a population size of 150 and maximum energy evaluations of 2.5×10^6. After 100 docking runs, cluster analysis with an RMS of 2.0 Å was used to find the most probable binding cluster.

2.8. Molecular dynamics simulation

Simulations of 200 nanoseconds (ns) were conducted on the non-complexed HPA (as control) and the HPA-water-soluble vitamin complexes using Gromacs 5.0 (Abraham, Murtola, Schulz, Páll, Smith, Hess, et al., 2015). An all-atom CHARMM27 force field was employed. SwissParam was used to generate the topologies for the water-soluble vitamins (Zoete, Cuendet, Grosdidier, & Michielin, 2011). The systems were placed in a rhombic dodecahedron (periodic box boundary = 1.2 nm), and TIP3P water model was used for solvation. System charges were neutralized, and, energy minimization with steepest descent algorithm was performed. The Berendsen thermostat, Parrinello–Rahman algorithm, and Particle Mesh Ewald methods were implemented for temperature, pressure coupling, and system electrostatics, respectively. Both van der Waal's cutoff and Coulomb interactions were set to 1 nm. All simulations were carried out at 310 K temperature and 1 bar pressure with $4.5e^{-5}$ bar^{-1} compressibility. The first two principal components (PC) of the trajectory were used for principal components analysis (Borah, Chakraborty, Jha, Rajkhowa, & Duary, 2016).

All amino acid residue numbering mentioned in the manuscript are according to published sequence data (Brayer, Luo, & Withers, 1995). Grace (http://plasma-gate.weizmann.ac.il/Grace/), PyMOL, and, Ligplot+ were used to plot the dynamics simulation trajectories, illustrate molecular images, and, visualize the 2D hydrogen/hydrophobic interactions, respectively.

2.9. Statistics

Fluorescence data were fitted using Matlab R2015b (The MathWorks, Inc., Natick, MA, USA). Analysis of variance (ANOVA) and Tukey's HSD post hoc analyses were conducted using SPSS 8.0 (SPSS, Inc., Chicago, IL, USA). Mean values were considered significantly different at $p < 0.05$.

3. Results and discussion

The inhibitory activity of eight water-soluble vitamins, namely, ascorbic acid, folic acid, pantothenic acid, thiamine, niacin, pyridoxine, biotin, and riboflavin was evaluated against human pancreatic α-amylase (HPA), and are shown in Fig. 1a. A significant inhibitory activity was exhibited by ascorbic acid and folic acid, followed loosely by pyridoxine. It is noteworthy that at the current experimental concentrations, the inhibitory activity of ascorbic acid is comparable to that of the reference inhibitor i.e. acarbose, the latter is a clinical antidiabetic drug. To examine this further, the IC_{50} was estimated using a non-linear sigmoidal fit (Fig. 1b). The model predicted IC_{50} of ascorbic acid was 1.54 ± 0.13 mg mL^{-1}. Ascorbic acid has been reported to show inhibitory activity against α-amylases, (Abell, Ratcliffe, & Gerrard, 1998) but IC_{50} values were not reported against HPA. We would like to point here that ascorbic acid was however less effective than acarbose. The IC_{50} of the latter was reported to be 6.90 ± 0.80 µg mL^{-1} (Yilmazer-Musa, Griffith, Michels, Schneider, & Frei, 2012). Also, we

estimated the IC_{50} of folic acid at 6.09 ± 0.26 mg mL^{-1}, therefore ca. five-folds less effective than ascorbic acid (IC_{50} result should be considered with precaution as folic acid demonstrates a competitive element later in the discussion). Additionally, IC_{50} of pyridoxine against HPA (IC_{50} result should be considered with precaution as the mode of inhibition is yet unknown) was seen to be 58.64 ± 0.40 mg mL^{-1} (data not shown). Noticeably, the reported IC_{50} values for folic acid (Shi, Wang, Zhang, Liu, & Fei, 2017) and pyridoxine (Kim, et al., 2018) are lower than our estimates. We believe this discrepancy arises from the differences in the structure of amylases used (Brayer, Luo, & Withers, 1995). The different substrate models (DQ starch in our case) could have also affected the IC_{50}. A partial dependence on the hydrogen bond formation amidst hydroxyl groups of small molecule ligands and amino acid residues within the active site of proteins has been contemplated necessary for small molecule-protein inhibitory activity (Lo Piparo, Scheib, Frei, Williamson, Grigorov, & Chou, 2008). Ascorbic acid and folic acid molecules contain four and two hydroxyl groups, respectively. This may be crucial in binding to HPA, leading to inhibition. In an agreement, the IC_{50} followed the order, ascorbic acid < folic acid (at the specified experimental substrate concentrations). However, pyridoxine consists of four hydroxyl groups. Likewise, pyridoxine should have had a comparable IC_{50} to ascorbic acid. This negates the above hypothesis, leading us to believe that the answers to the mechanism behind the five-fold higher inhibition of HPA by ascorbic acid (compared to folic acid) lay elsewhere. Niacin, Thiamine, Riboflavin, Pantothenic acid, and Biotin did not show any significant inhibition of HPA activity (cf. Fig. 1a).

Following these findings, we have thus focused on the inhibition kinetics, binding regime and the mechanism of inhibition of HPA by these two promising candidates, namely, ascorbic acid and folic acid using a range of complementary approaches.

3.1. Kinetics of HPA inhibition by ascorbic acid and folic acid

Michaelis-Menten plots (Fig. 2a, b) depicts the digestion of amylopectin corn starch by HPA in the presence and absence of ascorbic acid and folic acid. Additionally, the double-reciprocal Lineweaver-Burk plots of ascorbic acid and folic acid obtained from regression are presented in Fig. 2c, d. For ascorbic acid, the plots were observed to intersect near the x-axis on the second quadrant, providing initial evidence of a non-competitive mode of inhibition , whereas, for folic acid the intersection was achieved close to the y-axis, indicating a competitive mode of inhibition. Apart from this, K_m^{app} and V_{max}^{app} obtained by nonlinear fitting using the Michaelis-Menten equation shown in Table 1, gave further evidence for a non-competitive and competitive mode of inhibition for ascorbic acid and folic acid, respectively. The K_m^{app} value remained approximately constant and the V_{max}^{app} value decreased as the concentration of ascorbic acid was increased, indicating a non-competitive mode of inhibition (Proença, Freitas, Ribeiro, Sousa, Carvalho, Silva, et al., 2018). Contrarily, the K_m^{app} value increased and the V_{max}^{app} value remained constant as folic acid concentration increased, indicating a competitive mode of inhibition (Moon, Lee, Cho, Lee, Kim, & Ma, 2018).

Fig. 2e, g reveals that the Dixon and Eisenthal-Cornish-Bowden plots intersected at a single point for ascorbic acid. The K_{ic} and K_{in} values calculated from Eq. (4) and (5) were indicative of a non-competitive type of inhibition ($K_{ic} \simeq K_{in}$, cf. Table 1). An equality of K_{ic} and K_{in} has been reported necessary for a non-competitive antagonism (Hallek & Szinicz, 1988). For folic acid at various s, an intersection was observed close to the boundary of the first and the second quadrant for the plots of 1/v against i (Fig. 2f), whereas they were parallel in the plots for s/v against i (Fig. 2h). All pieces of evidence confirmed that folic acid was, in fact, a competitive inhibitor of HPA. Shi et al. (Shi, Wang, Zhang, Liu, & Fei, 2017) has indicated earlier through computational studies that folic acid exhibits a competitive element in the inhibition of porcine pancreatic α-amylase.

Additionally, we investigated if ascorbic acid and folic acid acted on the substrate to initiate any resistance to the enzyme digestion. It is widely accepted that the molecular packing order of starch dictates its digestion behaviour by amylases (Dhital, Warren, Butterworth, Ellis, & Gidley, 2017). In order to ascertain the absence of such artefacts, the heated substrate (to simulate cooking or processing) along with 2.5 and 20 mg mL^{-1} of ascorbic and folic acid (maximal inhibitor concentration used in section 2.4 for the detailed kinetic study), respectively were characterized using XRD. Amylopectin from corn starch used in the study is known to have an A-type molecular packing order, identifiable with 2θ angles at 15°, 17°, 18° and 23° (Borah, Rappolt, Duary, & Sarkar, 2019). However, the XRD diffractograms of the heated substrate and the heated substrate mixed with the water-soluble vitamins show a total lack of any diffraction contribution (Fig. S1). We propose that heating starch at the experimental conditions should lead to gelatinization of the substrate, resulting in the total loss of the A-type molecular packing order. It is widely accepted that gelatinization results in structural destructuring of starch (Chen, Tian, McClements, Huang, Zhu, Wang, et al., 2019). It is of note that, this destructuring in the molecular packing order did not recover or alter in any way, by the presence of ascorbic acid or folic acid during experimentation. Therefore, it may be safe to state that ascorbic and folic acid did not act on the substrates to resist enzymatic hydrolysis.

3.2. Binding interactions of ascorbic acid and folic acid to HPA

At 300 K, an increase in λ_{em}^{max} was observed upon increasing the concentration (i) of ascorbic acid till 0.001 mg mL^{-1}. This subsequently decreases as the concentration of ascorbic acid was further increased to 0.01 mg mL^{-1} (Fig. S2a). Contrarily, at 300 K, the decay-associated λ_{em}^{max} for folic acid appeared to be concentration-dependent (Fig. S2d). The former was true in the case of both ascorbic acid and folic acid at 310 K (Fig. S2b, e). We postulate an increase in the burial of tryptophan (Trp) residues (decreasing the solvent-accessibility of Trp) arising

from tighter protein folding upon ascorbic acid and folic acid binding, lead to the increased λ_{em}^{max} at low i. However, the systematic quenching of fluorescence in HPA at higher concentrations of ascorbic acid and folic acid should be due to Trp residues becoming more solvent accessible. Similar observations were made in the cases of the unfolded protein state of Brugia malayi Glucose 6-phosphate dehydrogenase upon cofactor $NADP^+$ binding (Verma, Chandra, Suthar, Doharey, Siddiqi, & Saxena, 2016). This unfolding of the protein structure can well describe the reduction in enzymatic activity. Additionally, a 5 nm and 6 nm redshifts at λ_{em}^{max} were observed for folic acid quenched HPA at 300 K and 310 K, respectively (Fig. S2d, e). This might be attributed to an unfolded protein state with higher solvent-accessibility for Trp. As for example in other experiments, free L-Trp amino acid residues (Fig. S2g, h) were redshifted by ca. > 35 nm. Thus, the definition holds true in our case, as was known that λ_{em}^{max} for Trp ranges from ca. 308 nm in comparatively nonpolar environments to λ_{em}^{max} of ca. 350 nm in polar solvents like water (Vivian & Callis, 2001). Interestingly, the greater redshift of λ_{em}^{max} for folic acid bound HPA at 310 K (physiological temperature), indicated greater protein unfolding at elevated temperatures. Although very subtle, the inhibition mechanism could thereby be dependent on temperature.

The fluorescence data were fitted to the classical Stern-Volmer equation, $\frac{F_o}{F_{corr}} = 1 + k_q \tau_o [i] = 1 + K_{SV}[i]$ to describe the fluorescence quenching behavior. Here, F_o and F_{corr} were the intensities of fluorescence in the presence and absence of i, respectively; k_q was the bimolecular quenching constant; and τ_o was the average lifetime of the fluorophore in the unquenched excited-state (for α-amylase, τ_o would be 2.97 ns). The K_{sv} was the Stern-Volmer quenching constant. For ascorbic acid, a linear Stern-Volmer plot was observed. This extrapolated to a static quenching mechanism of the Trp fluorophore in HPA. On the contrary, folic acid exhibited an upward curve, indicating a plausible interplay of a dynamic as well as static companion quenching mechanism. Also, the probability of quenching via the

establishment of a sphere of action mechanism cannot be ruled out at this stage. Therefore, for both ascorbic acid (Fig. S2c) and folic acid (Fig. S2f), considering that the fluorescence quenching followed the apparent static quenching conformation of the Stern-Volmer equation narrating the sphere of action model, the data were described as, $\frac{F_o}{F_{corr}} = e^{(K_{FQ}[i])}$ (Sun, Chen, Meng, Yang, Yuan, & Guo, 2016). Here, K_{FQ} was the apparent static quenching constant. Additionally, the binding parameters of ascorbic acid and folic acid with HPA were estimated as, $\log\left(\frac{F_o - F_{corr}}{F_{corr}}\right) = n\log[i] - nlogK_{diss}$, where F_{corr} and F_o are the intensities of fluorescence of HPA in the presence and absence of ascorbic acid and folic acid. The number of water-soluble vitamin binding sites (n) was estimated from the slope of the double logarithmic plot of the experimental data. The binding constant K_A was estimated from the reciprocal of K_{diss}, which was a logarithm of log [i] at log $[(\frac{F_o - F_{corr}}{F_{corr}})] = 0$.

Comparing Table 1 and 2, we observed that the number of binding sites per molecule of HPA (n, where ascorbic acid > folic acid) were in correspondence with the association constant ($\frac{1}{K_{ic}}$, where ascorbic acid > folic acid). Note, K_{ic} (from Table 1) was indicative of the dissociation of the HPA-water-soluble vitamin complex, while the reciprocal value indicates an association constant (Sun, Chen, Meng, Yang, Yuan, & Guo, 2016). The plot of $1/V_{max}^{app}$ against [i] was seen as a parabolic curve (Fig. S3), which suggests binding of multiple inhibitor molecules per molecule of the enzyme. Although n may refer to identical binding sites per molecule of enzyme, i.e. binding of an inhibitor to identical sites on the same enzyme can occur independently. However, in our case, the parabolic curve points to the existence of multiple inhibition sites that are not identical. Previously, other researchers (Gou, Lü, Park, Oh, Shi, Park, et al., 2008; Park, Lee, Park, Kim, Hahn, & Yang, 2003) have discussed similar findings in the parabolic non-competitive type of antagonism of tyrosinase activity by

bromoacetate, dithiothreitol and β-mercaptoethanol. We hereby propose that, the higher per enzyme binding nature of ascorbic acid to HPA at independent allosteric binding sites (as compared to folic acid), allows the former to interact significantly with HPA. In this scenario, multiple ascorbic acid molecules can contribute more hydroxyl groups in formation of hydrogen bonds with amino acid residues in the allosteric binding pockets of HPA. Thus, leading to alterations in the enzyme conformation which are unfavorable for optimal activity. This explains the ca. five-fold higher inhibition potential of ascorbic acid compared to that of folic acid.

The binding forces were estimated as, $ln\frac{K_{A_{310}}}{K_{A_{300}}} = \frac{\Delta H^O}{R}(\frac{1}{T_{300}} - \frac{1}{T_{310}})$, $\Delta G^o = -RTlnK_A$, and, $\Delta S^o = \frac{\Delta H^O - \Delta G^O}{T}$, and are shown in Table 2. Here, T was the system temperature in Kelvin (K), and, R was the gas constant (8.314 J mol^{-1} K^{-1}). In our estimations, ΔH^o (enthalpy change) < 0 and ΔS^o (entropy change) > 0 for both ascorbic acid and folic acid are suggestive of hydrophobic interaction, van der Waals forces or formation of hydrogen bonds, respectively. The association process was spontaneous, revealed by ΔG^o (free energy change) < 0.

3.3. Förster resonance energy transfer (FRET) estimates

Since our measurement wavelength (λ) was in nm, the critical Förster distance corresponding to the donor-acceptor distance (in Å) for 50% FRET efficiency was described as $R_o = (0.211)\left(\sqrt[6]{\frac{\kappa^2\phi_D}{{r_i}^4}J(\lambda)}\right)$. Here, κ^2 was the donor-acceptor orientation factor at 0.476 (Steinberg, 1971), r_i was the refractive index of buffered salts at 1.4, ϕ_D was the donor's fluorescence quantum yield in water at 23ºC in absence of the acceptor at 0.13 (R. F. Chen, 1967). Here, J(λ) was the overlap integral amidst the normalized absorption spectra of the acceptor and the emission spectra of the donor (Fig. S4), defined in $M^{-1}cm^{-1}nm^4$. The value

of $J(\lambda)$ equaled to $\int_0^\infty \varepsilon_A(\lambda)\,\lambda^4 F_D(\lambda)d\lambda$. Here, $\varepsilon_A(\lambda)$ was the spectra for the extinction coefficient of the acceptor ($M^{-1}cm^{-1}$), and $F_D(\lambda)$ was the wavelength dependent normalized donor emission spectrum. The energy transfer efficiency (E) component and the apparent distance in Å (r^{app}) amidst the donor-acceptor were described as, $E = 1 - \frac{F_{corr}}{F_o}$, and, $r^{app} = \sqrt[6]{\frac{R_o^6}{E} - R_o^6}$. As seen from Table S1, FRET was highly unlikely in the case of ascorbic acid and Trp residues of HPA ($R_o < r^{app}$). However, there was a high likelihood of FRET between folic acid and Trp residues of HPA ($R_o > r^{app}$). FRET between folic acid and Trp residues of porcine pancreatic α-amylase has been reported earlier (Shi, Wang, Zhang, Liu, & Fei, 2017). FRET also explains the greater decrease in λ_{em}^{max} and the 6 nm redshift observed in the previous section for the HPA-folic acid complex. FRET has been reported to result in a redshift of λ_{em}^{max} (Wu, Wang, Dai, Miao, & Zhao, 2016). The researchers observed FRET between coumarin and a 2-dicyanomethylene-3-cyano-4,5,5-trimethyl-2,5-dihydrofuran fluorophore, resulting in a redshift. K_{FQ} and k_q were in agreement to FRET for both ascorbic acid and folic acid.

3.4. Molecular docking studies and molecular dynamics simulation

Molecular docking predicted that ascorbic acid could be located in two independent binding pockets (referred to as site 1 and site 2). The most frequent cluster of binding to HPA and the hydrogen bond interactions are shown in Fig. S5a, b, d, e. The docking study also ascertains the parabolic non-competitive inhibition that is usually realized when there exist multiple inhibitor binding sites. The corresponding free energy of binding (ΔG_{dock}^o) for ascorbic acid at both site 1 and site 2 are in Table S2. Notably, the results were in agreement to the parameter estimated through fluorescence studies, especially corroborating well with n, ΔH^o, ΔG^o and ΔS^o (cf. Table 2). The difference in terms of the actual numerical values of ΔG_{dock}^o and ΔG^o was a resultant of the lack of solvation during docking. As such, conformational changes in

the structure of HPA was probed using molecular dynamics simulation to study the properties arising from unanticipated conformational scrambling in the polypeptide structure, in response to ascorbic acid binding.

The HPA with two ascorbic acid molecules bound at site 1 and site 2 were simulated for 200 nanoseconds in water, corresponding to the n values and molecular docking cluster analysis. The r^{app} distance of ascorbic acid (cf. Table S1) showed compliance to the computationally calculated average value of 1.34 ± 0.15 nm for both site 1 and site 2 (data not shown), confirming the accuracy of the computation. The ascorbic acid molecules formed interactions along with the protein surface through an average of ca. > six hydrogen bond (Fig. S6c). The lowest energy structure was extracted from the simulation ensemble by free energy landscape (FEL) analysis using the principal components, PC1 and PC2 (Fig. S7a). It was interesting to observe that both the allosteric binding sites are located distant (> ca. 1 nm) from the catalytic cavity of the enzyme, particularly, site 2 being opposite to the elongated active site cavity housing the key conserved active site residues Asp^{197}, Glu^{233}, and Asp^{300}. These active carboxylic acid residues hydrolyze the α-1, 4-linked glucose subunits in the starch chain via a double displacement mechanism (Li, Begum, Numao, Park, Withers, & Brayer, 2005). The residue Asp^{197} is known to act as a catalytic nucleophile, whereas Glu^{233} acts as an acid/base catalyst (Rydberg, Li, Maurus, Overall, Brayer, & Withers, 2002). The residue Asp^{300} is known to be part of the hinge region of the mobile and conserved loop 7 (residues 295-315) that flanks the active site cavity (Andre & Tran, 2004). Hydrogen bonding with HPA residues are shown in Fig. S8 and Fig. S9. Despite this remote binding, the dual ascorbic acid molecules resulted in significant conformational scrambling represented as B-factor fluctuations in segments located near the active site cleft. Compared to the non-complexed HPA, increased disorder was observed in loop 8 (residues 346-353), and increased order was observed in loop 3 (residues 105-111), loop 6 (residues 235-243), and loop 7

(residues 295-315), respectively (Fig. 3a, b, d**)**. Loop 3 is generally acknowledged to contribute to substrate binding residues for the subsites (1 to 5) on either side of the elongated active site cavity (MacGregor, 1993). For optimal HPA catalysis, a segment of glucose in starch needs to occupy five neighboring subsites (1 to 5) in this elongated cavity (Butterworth, Warren, & Ellis, 2011; MacGregor, 1993). These subsites are each capable of binding one glucose unit in the starch chain. This cavity lies on the C-terminal end section of eight parallel β-strands that make up the framework for a triose-phosphate isomerase (TIM) barrel. This is a conserved protein fold that consisting of eight additional α-helices which occur in turn repeatedly along the polypeptide backbone (Brayer, Luo, & Withers, 1995). Intuitively, an increased order will hinder proper loop 3 functionality, limiting catalysis. Additionally, upon substrate binding, loop 7 is known to flip over the active site cavity, locking the substrate in place, and positioning Asp^{300} into a catalytic position closer to Asp^{197} and Glu^{233} (Andre & Tran, 2004). This is described as the closed position for loop 7. Contrarily, an open position is reached in the absence of substrate binding, with the loop flipping again in the opposite direction. The largest displacement between the closed and open positions is reported to be ca. 0.6 nm for the residue His^{305} in loop 7 (Andre & Tran, 2004). In our case, loop 7 was only displaced by a magnitude of ca. $^1/_2$ orders than the non-complexed protein as seen in Fig. S11b, a. The lower RMSD of the ascorbic acid-complexed HPA, compared to that of the non-complexed form confirms the enhanced stability (Fig. S6a). Remarkably, the active site residue Asp^{300} (part of loop 7 hinge region) was installed closer (1.05 ± 0.08 nm) to the residues Asp^{197} and Glu^{233} (Fig. S6b). The limited loop 7 displacement, accompanied by a tighter congruence of the residues Asp^{197}, Glu^{233}, and Asp^{300}, and, the enhanced loop 3 order, appears to be largely responsible for giving rise to a sterically unfavorable binding cavity for starch chains. To verify this hypothesis, maltopentaose was docked into the active site cavity of the FEL frame of the HPA-ascorbic acid complex (for chronological continuity with

experiments). A ΔG^{o}_{dock} value of -5.22 kcal mol^{-1} was estimated, which was far less than that estimated for non-complexed HPA (-8.47 kcal mol^{-1}). It has been reported previously that experimental ΔG values become more negative (from ca. -5 to -16 KJ mol^{-1}) as the subsites 1-5 of porcine pancreatic α-amylase fills with glucose residues of a substrate (Seigner, Prodanov, & Marchis-Mouren, 1987; Seigner, Prodanov, & Marchis-Mouren, 1985). Similarly, it was worth noting in our case, that the total free energy of binding accruing from occupancy of the non-complexed HPA active site was a consequence arising from occupancy of the five sub-sites (1 to 5) filled with glucose residues in maltopentaose (Fig. S12a), which was the optimal catalytic condition for HPA. However, in the case of HPA-ascorbic acid complex, steric distortions within the active site cavity led to substrate binding, where the series of glucose residues could not fill the five subsites (cf. Fig. S12b). Likewise, a substrate that does not bind securely to the active site cannot undergo optimal hydrolysis.

A closer inspection of the binding revealed that the ascorbic acid allosteric binding site 1 was situated along the pocket formed by the crossover connections between helix α-3 and loop 2, 3 (Fig. 4a). Here, ascorbic acid forms a hydrogen bond with the residue Glu^{181} and hydrophobic interactions with residue Tyr^{182} located along helix α-3. Additional, hydrophobic interactions with residues Tyr^{67} and Lys^{68} located along the loop 2 were achieved. The proximity of site 1 to helix α-3, that eventually connect to the observed ordered loop 3 regions was indicative that this can be partly the ordering mechanism via which ascorbic acid exerts its inhibition effect on the subsites in the cavity. Additionally, at the ascorbic acid allosteric binding site 2, hydrogen bonds are formed with the residue Arg^{398} and Asp^{402}, both positioned along the helix α-8 (Fig. 4a). An additional hydrogen bond interaction was formed with the residue Arg^{421}, part of a β-sheet in the C-domain. Apart from that, hydrophobic interactions were established with residue Thr^{11} located along the strand of the polypeptide chain, leading up to β-sheet 1. Hydrophobic interactions were also established with the residues Pro^{332},

Gly[334], and Phe[335] located along the polypeptide loop housed between helix α-7 and β-sheet 8. All bonded interactions are shown in Fig. S8 and Fig. S9. Here, the ordering in loop 7 was expected to be caused by β-sheet 7 and helix α-7 (Fig. 4). Contrarily, the involvement of the β-sheet 7 and helix α-8 leading towards the C-terminal end was expected to cause the disorder in loop 8. Since, both the scrambled segments rail between the β-strands and the helices, a particular participation of β-sheet 7 and helices α-7, α-8 are proposed (Fig. 4a).

From the findings, it can be said that ascorbic acid constitutes a class of allosteric inhibitors that can operate remotely and induces exceptionally specific polypeptide chain conformational scrambling in the neighborhood of the active site cavity of HPA. Ascorbic acid was situated very close to the β-sheets and helices that eventually bridge to the regions exhibiting the scrambling. Seemingly, the effect was channeled through the TIM barrel, from one end of the geometry towards the C-terminal end of the parallel β-strands of the barrel housing the three active site residues within the elongated substrate binding cavity. It was fascinating that ascorbic acid governs this dynamic scrambling via interactions with just ca. seven residues. Experimental evidence of a similar mechanism of inhibition of HPA by ethyl caffeate has been reported previously (Williams, Li, Withers, & Brayer, 2012). Similar to our observations, the bound ethyl caffeate was observed to act via the TIM barrel, and precisely induce disordering in the polypeptide chain segments forming the elongated substrate binding cavity.

On the other hand, molecular docking predicted folic acid to be located within the elongated substrate binding active site cavity of HPA. This indicated a competitive mechanism of inhibition, in agreement with the experimental results. The corresponding free energy of binding (ΔG^{o}_{dock}), and, the most likely binding cluster and the hydrogen bonding in the HPA-folic acid complex are shown in Table S2, and Fig. S5c, f, respectively. The docking

results were in agreement to the parameter estimated through fluorescence studies (n, ΔH^o, ΔG^o, *and* ΔS^o) (cf. Table 2).

The HPA-folic acid structure was simulated for 200 nanoseconds in water, and the pteridine and the p-aminobenzoic acid moiety of folic acid was seen to be positioned very close to the residue Trp^{58} and Trp^{59}, respectively (0.55 ± 0.08 nm) throughout the simulation time (data not shown). This was in close agreement with r^{app} (cf. Table S1). The molecule interacted with the protein surface through an average of ca. > four hydrogen bond interactions (Fig. S6d) throughout the simulation time. The lowest energy structure was extracted from the simulation ensemble by FEL analysis (Fig. S7b). We observed that the hydrophobic pteridine moiety of folic acid orients into the +4 subsite to form a hydrogen bond with Asp^{300} (Fig. S10). Also, hydrophilic glutamyl end of folic acid lies parallel to the elongated substrate binding cavity of HPA (subsites 1 to 3). This should negate substrate binding into the elongated substrate binding cavity. Additionally, the O-atom in the pteridine moiety of folic acid established a hydrogen bond with the putative nucleophilic water molecule positioned along the side chain of residue Glu^{233}, functionally locking it (Fig. S10, and Fig. S13). This water molecule is known to play a predominant role in the latter half of the starch hydrolysis reaction (Rydberg, Li, Maurus, Overall, Brayer, & Withers, 2002). Comparing the present binding mode to the docking frame (Fig. S5f**)**, a distinctive feature for discourse was the mannerism of folic acid binding, where the spatial disputes play out resulting in loss of hydrogen bonding with the other active site residues Asp^{197} and Glu^{233}, due to the shift in the placement of the loop 7 (His^{305} Cα displacement of 0.55 nm, Fig. S11c). Folic acid binding ushers a reduction in B-factor fluctuations in segments neighboring the active site cavity, namely, loop 3 (residues 105-111) and loop 8 (residues 346-353 and residues 363-366) as seen in Fig. 3c, d. This brings about stability in the overall structure of HPA, seen through the reduction of RMSD (Fig. S6a). Regardless, folic acid attaches to the

active binding cavity and manages to disturb the nearby conformation of the polypeptide chains. Interestingly, loop 7 was only partially ordered (ca. 70%). Ordering was confined to residues 295-299 and 306-315 (cf. loop 7 residues 295-315 are 20 in total). As seen in Fig. 3c, d, a disordering was also observed in Loop 6 (residues 235-243). Note, the folic acid-induced disorder was confined only around the elongated catalytic cavity (Fig. 3c). The vicinity of this cavity houses ca. five Trp residues that were disordered, and this can partly explain the ca. 6 nm red shift in λ_{em}^{max} observed during the fluorescence studies. Amidst this conformational scrambling, the active site residue Asp^{300} had installed closer (compared to the non-complexed HPA) with an average distance of 1.16 ± 0.07 nm from the residues Asp^{197} and Glu^{233} (Fig. S6b), strutted by hydrogen bonding with folic acid (Fig. S10). This should translate into a catalytically unproductive active site space. This hypothesis was again verified using a maltopentaose molecule, as described for ascorbic acid. A ΔG_{dock}^{o} value of -6.88 kcal mol^{-1} was estimated, which was lesser than non-complexed HPA (Fig. S12c).

Folic acid forms one hydrogen bond with the active site residue Asp^{300}, leading to the observed partial ordering of loop 7. Hydrophobic interactions with residue Ala^{106} also seems to diminish the disorder along loop 3. Additionally, hydrophobic interactions were realized with residues Asn^{53}, Trp^{58} and Trp^{59} located along loop 2, the latter is housed between the β-sheet 2 and helix α-3 (cf. Fig. 4b). The proximity of loop 2 polypeptide chain (specifically the bulky residues, Trp^{58}, and Trp^{59}) to the loop 8 (specifically the bulky residues $Trp^{357, 358, 359}$) could possibly result in steric destabilization leading to the observed heightened disorder of loop 8 (cf. Fig. 3c, and Fig. 4). All bonding interactions are shown in Fig. S10. Note, the role of loop 6 and 8 in the catalytic activity of HPA is not well established, and therefore it was hard to make assumptions about their role in our case. The role of loop 6 and 8 deserves further attention.

4. Conclusion

This work is the first step towards uncovering the potential of eight water-soluble vitamins to slow-down starch digestion via inhibition of human pancreatic α-amylase (HPA) activity. This mechanistic study reveals in particular two promising water-soluble vitamin candidates, namely, ascorbic acid and folic acid. The experimental results were in agreement to the computational studies, with the latter elucidating the structural mechanism of inhibition via remarkable conformational scrambling of the polypeptide chains in the HPA structure. Ascorbic acid revealed as a category of allosteric inhibitors with a mode of exertion that operates remotely from the active site cavity and induces exceptionally specific polypeptide chain conformational scrambling in the neighborhood of the active site cavity of HPA. Seemingly, the effect was channeled through the TIM barrel. Furthermore, folic acid binds to and then negates the functionality of Asp^{300} by creating steric conflicts for substrate binding in the active site cavity. This was proposed to offset the catalytic nucleophile and acid/ base functionality. This was remarkable, and such competitive inhibition is rarely observed, except for other substrate-mimicking inhibitors like acarbose. Notably, the relatively weak IC_{50} would limit the usefulness of ascorbic acid and folic acid against HPA, nevertheless, their activity may be improved by possibly studying the dual effect as associate inhibitors. This aspect needs further exploration and may be a step towards comprehending HPA catalysis in heterogeneous inhibitor conditions. Fundamental insights from this study provide a structural basis for infusing starch with biocompatible and nutritional water-soluble vitamins to enable slow postprandial increment in blood glucose levels and thus offer exciting avenues for designing food and pharmaceutical applications targeting diabetes management.

Acknowledgements

PKB is a Commonwealth Scholar funded by the UK government. The authors want to thank the Advanced Research Computing facility, University of Leeds and the High Performance Computing Centre, Tezpur University for use of the ARC2 and PARAM Shavak, respectively. Dr. Rupak Mukhapadhyay, Dr. Suman Dasgupta, Mr. Anindhya Sundar Das, Mr. Dipanjan Banerjee (Department of Molecular Biology and Biotechnology, Tezpur University) and Mr. Prakash Kurmi (Sophisticated Analytical Instrumentation Centre, Tezpur University) are duly acknowledged for their technical support in spectrophotometry, spectrofluorimetry, and XRD.

Conflict of interest

The authors declare no conflict of interests.

References

Abell, A. D., Ratcliffe, M. J., & Gerrard, J. (1998). Ascorbic acid-based inhibitors of α-amylases. Bioorganic & medicinal chemistry letters, 8(13), 1703-1706. https://doi.org/10.1016/S0960-894X(98)00298-4.

Abraham, M. J., Murtola, T., Schulz, R., Páll, S., Smith, J. C., Hess, B., & Lindahl, E. (2015). GROMACS: High performance molecular simulations through multi-level parallelism from laptops to supercomputers. SoftwareX, 1-2, 19-25. https://doi.org/10.1016/j.softx.2015.06.001.

Andre, G., & Tran, V. (2004). Putative implication of α-amylase loop 7 in the mechanism of substrate binding and reaction products release. Biopolymers, 75(2), 95-108. https://doi.org/10.1002/bip.20096.

Borah, P. K., Chakraborty, S., Jha, A. N., Rajkhowa, S., & Duary, R. K. (2016). In silico approaches and proportional odds model towards identifying selective ADAM17

inhibitors from anti-inflammatory natural molecules. Journal of Molecular Graphics and Modelling, 70, 129-139. https://doi.org/10.1016/j.jmgm.2016.10.003.

Borah, P. K., Rappolt, M., Duary, R. K., & Sarkar, A. (2019). Effects of folic acid esterification on the hierarchical structure of amylopectin corn starch. Food Hydrocolloids, 86, 162-171. https://doi.org/10.1016/j.foodhyd.2018.03.028.

Brayer, G. D., Luo, Y., & Withers, S. G. (1995). The structure of human pancreatic α-amylase at 1.8 Å resolution and comparisons with related enzymes. Protein Science, 4(9), 1730-1742. https://doi.org/10.1002/pro.5560040908.

Butterworth, P. J., Warren, F. J., & Ellis, P. R. (2011). Human α-amylase and starch digestion: An interesting marriage. Starch-Stärke, 63(7), 395-405. https://doi.org/10.1002/star.201000150.

Chen, L., Tian, Y., McClements, D. J., Huang, M., Zhu, B., Wang, L., Sun, B., Ma, R., Cai, C., & Jin, Z. (2019). A simple and green method for preparation of non-crystalline granular starch through controlled gelatinization. Food Chemistry, 274, 268-273. https://doi.org/10.1016/j.foodchem.2018.09.006.

Chen, R. F. (1967). Fluorescence quantum yields of tryptophan and tyrosine. Analytical Letters, 1(1), 35-42. https://doi.org/10.1080/00032716708051097.

Dhital, S., Warren, F. J., Butterworth, P. J., Ellis, P. R., & Gidley, M. J. (2017). Mechanisms of starch digestion by α-amylase—Structural basis for kinetic properties. Critical reviews in food science and nutrition, 57(5), 875-892. https://doi.org/10.1080/10408398.2014.922043.

Gayen, A., Chatterjee, C., & Mukhopadhyay, C. (2008). GM1-induced structural changes of bovine serum albumin after chemical and thermal disruption of the secondary structure: a spectroscopic comparison. Biomacromolecules, 9(3), 974-983. https://doi.org/10.1021/bm701144k.

Gonçalves, C., Rodriguez-Jasso, R. M., Gomes, N., Teixeira, J. A., & Belo, I. (2010). Adaptation of dinitrosalicylic acid method to microtiter plates. Analytical Methods, 2(12), 2046-2048. https://doi.org/10.1039/C0AY00525H.

Gou, L., Lü, Z.-R., Park, D., Oh, S. H., Shi, L., Park, S. J., Bhak, J., Park, Y.-D., Ren, Z.-L., & Zou, F. (2008). The Effect of Histidine Residue Modification on Tyrosinase Activity and Conformation: Inhibition Kinetics and Computational Prediction. Journal of Biomolecular Structure and Dynamics, 26(3), 395-401. https://doi.org/10.1080/07391102.2008.10507254.

Hallek, M., & Szinicz, L. (1988). Effects of some mono-and bisquaternary ammonium compounds on the reactivatability of soman-inhibited human acetylcholinesterase in vitro. Biochemical pharmacology, 37(5), 819-825. https://doi.org/10.1016/0006-2952(88)90167-0.

Kato-Schwartz, C. G., Bracht, F., Gonçalves, G. d. A., Soares, A. A., Vieira, T. F., Brugnari, T., Bracht, A., & Peralta, R. M. (2018). Inhibition of α-amylases by pentagalloyl glucose: Kinetics, molecular dynamics and consequences for starch absorption. Journal of Functional Foods, 44, 265-273. https://doi.org/10.1016/j.jff.2018.03.025.

Kim, H. H., Kang, Y. R., Lee, J. Y., Chang, H. B., Lee, K. W., Apostolidis, E., & Kwon, Y. I. (2018). The Postprandial Anti-Hyperglycemic Effect of Pyridoxine and Its Derivatives Using In Vitro and In Vivo Animal Models. Nutrients, 10(3), 285-296. https://doi.org/10.3390/nu10030285.

Li, C., Begum, A., Numao, S., Park, K. H., Withers, S. G., & Brayer, G. D. (2005). Acarbose rearrangement mechanism implied by the kinetic and structural analysis of human pancreatic α-amylase in complex with analogues and their elongated counterparts. Biochemistry, 44(9), 3347-3357. https://doi.org/10.1021/bi048334e.

Lo Piparo, E., Scheib, H., Frei, N., Williamson, G., Grigorov, M., & Chou, C. J. (2008). Flavonoids for controlling starch digestion: structural requirements for inhibiting human α-amylase. Journal of medicinal chemistry, 51(12), 3555-3561. https://doi.org/10.1021/jm800115x.

MacGregor, E. A. (1993). Relationships between structure and activity in the α-amylase family of starch-metabolising enzymes. Starch-Stärke, 45(7), 232-237. https://doi.org/10.1002/star.19930450705.

Mason, S., Rasmussen, B., & Wadley, G. D. (2018). Ascorbic Acid Supplementation Improves Postprandial Glucose and Blood Pressure in People with Type 2 Diabetes. Diabetes, 67(Supplement 1), 206. https://doi.org/10.2337/db18-789-P.

Miller, G. L. (1959). Use of dinitrosalicylic acid reagent for determination of reducing sugar. Analytical chemistry, 31(3), 426-428. https://doi.org/10.1021/ac60147a030.

Moon, K. M., Lee, B., Cho, W.-K., Lee, B.-S., Kim, C. Y., & Ma, J. Y. (2018). Swertiajaponin as an anti-browning and antioxidant flavonoid. Food Chemistry, 252, 207-214. https://doi.org/10.1016/j.foodchem.2018.01.053.

Morris, G. M., Huey, R., Lindstrom, W., Sanner, M. F., Belew, R. K., Goodsell, D. S., & Olson, A. J. (2009). AutoDock4 and AutoDockTools4: Automated docking with selective receptor flexibility. Journal of computational chemistry, 30(16), 2785-2791. https://doi.org/ 10.1002/jcc.21256.

Neese, F. (2012). The ORCA program system. Computational Molecular Science, 2(1), 73-78. https://doi.org/10.1002/wcms.81.

Park, Y.-D., Lee, S.-J., Park, K.-H., Kim, S.-y., Hahn, M.-J., & Yang, J.-M. (2003). Effect of Thiohydroxyl Compounds on Tyrosinase: Inactivation and Reactivation Study. Journal of Protein Chemistry, 22(7), 613-623. https://doi.org/10.1023/B:JOPC.0000008726.99095.48.

Proença, C., Freitas, M., Ribeiro, D., Sousa, J. L. C., Carvalho, F., Silva, A. M. S., Fernandes, P. A., & Fernandes, E. (2018). Inhibition of protein tyrosine phosphatase 1B by flavonoids: A structure - activity relationship study. Food and Chemical Toxicology, 111, 474-481. https://doi.org/10.1016/j.fct.2017.11.039.

Rydberg, E. H., Li, C., Maurus, R., Overall, C. M., Brayer, G. D., & Withers, S. G. (2002). Mechanistic analyses of catalysis in human pancreatic α-amylase: Detailed kinetic and structural studies of mutants of three conserved carboxylic acids. Biochemistry, 41(13), 4492-4502. https://doi.org/10.1021/bi011821z.

Seigner, C., Prodanov, E., & Marchis-Mouren, G. (1987). The determination of subsite binding energies of porcine pancreatic α-amylase by comparing hydrolytic activity towards substrates. Biochimica et Biophysica Acta, 913(2), 200-209. https://doi.org/10.1016/0167-4838(87)90331-1.

Seigner, C., Prodanov, E., & Marchis-Mouren, G. (1985). On porcine pancreatic α-amylase action: kinetic evidence for the binding of two maltooligosaccharide molecules (maltose, maltotriose and o-nitrophenylmaltoside) by inhibition studies: Correlation with the five-subsite energy profile. European journal of biochemistry, 148(1), 161-168. https://doi.org/10.1111/j.1432-1033.1985.tb08820.x.

Shi, W., Wang, Y., Zhang, H., Liu, Z., & Fei, Z. (2017). Probing deep into the binding mechanisms of folic acid with α-amylase, pepsin and trypsin: An experimental and computational study. Food Chemistry, 226, 128-134. https://doi.org/10.1016/j.foodchem.2017.01.054.

Spoelstra-de Man, A. M. E., Elbers, P. W. G., & Oudemans-Van Straaten, H. M. (2018). Vitamin C: should we supplement? Current Opinion in Critical Care, 24(4), 248-255. https://doi.org/10.1097/MCC.0000000000000510.

Steinberg, I. Z. (1971). Long-range nonradiative transfer of electronic excitation energy in proteins and polypeptides. Annual review of biochemistry, 40(1), 83-114. https://doi.org/10.1146/annurev.bi.40.070171.000503.

Sun, L., Chen, W., Meng, Y., Yang, X., Yuan, L., & Guo, Y. (2016). Interactions between polyphenols in thinned young apples and porcine pancreatic α-amylase: Inhibition, detailed kinetics and fluorescence quenching. Food chemistry, 208, 51-60. https://doi.org/10.1016/j.foodchem.2016.03.093.

Verma, A., Chandra, S., Suthar, M. K., Doharey, P. K., Siddiqi, M. I., & Saxena, J. K. (2016). NADP+ binding effects tryptophan accessibility, folding and stability of recombinant B. malayi G6PD. International journal of biological macromolecules, 85, 645-654. https://doi.org/10.1016/j.ijbiomac.2015.12.087.

Vivian, J. T., & Callis, P. R. (2001). Mechanisms of tryptophan fluorescence shifts in proteins. Biophysical journal, 80(5), 2093-2109. https://doi.org/10.1016/S0006-3495(01)76183-8.

Williams, L. K., Li, C., Withers, S. G., & Brayer, G. D. (2012). Order and disorder: differential structural impacts of myricetin and ethyl caffeate on human amylase, an antidiabetic target. Journal of medicinal chemistry, 55(22), 10177-10186. https://doi.org/10.1021/jm301273u.

Wu, W. L., Wang, Z. Y., Dai, X., Miao, J. Y., & Zhao, B. X. (2016). An effective colorimetric and ratiometric fluorescent probe based FRET with a large Stokes shift for bisulfite. Scientific reports, 6, 25315-25320. https://doi.org/10.1038/srep25315.

Yilmazer-Musa, M., Griffith, A. M., Michels, A. J., Schneider, E., & Frei, B. (2012). Grape seed and tea extracts and catechin 3-gallates are potent inhibitors of α-amylase and α-glucosidase activity. Journal of agricultural and food chemistry, 60(36), 8924-8929. https://doi.org/10.1021/jf301147n.

Zoete, V., Cuendet, M. A., Grosdidier, A., & Michielin, O. (2011). SwissParam: a fast force field generation tool for small organic molecules. Journal of computational chemistry, 32(11), 2359-2368. https://doi.org/10.1002/jcc.21816.

Figure Captions:

Fig. 1. Initial reaction velocity of amylopectin corn starch digestion by HPA in the presence and absence of eight water-soluble vitamins and acarbose (reference inhibitor) (a). [a, b, c] Data are significantly different within the group ($p < 0.05$, Tukey's HSD Post Hoc analysis). Fitting

of using Eq. (2) for the calculation of IC_{50} of ascorbic acid (▲) and folic acid (■) (b). The data were presented as the means ± standard deviations. Axis labels indicate, reaction velocity (v), and, water-soluble vitamin (inhibitor) concentrations (i).

Fig. 2. Michaelis-Menten, Lineweaver-Burk, Dixon, and Eisenthal-Cornish-Bowden plots for ascorbic acid (a, c, e, g), and, folic acid (b, d, f, h), respectively. The data were presented as the means ± standard deviations for the Michaelis-Menten plots. Different concentrations of the water-soluble vitamins are listed in the legend entries. 0 mg mL^{-1} represents amylopectin corn starch digestion with PBS buffer (control) without the addition of water-soluble vitamins. Axis labels indicate, substrate concentration (s), reaction velocity (v), and, water-soluble vitamin (inhibitor) concentrations (i).

Fig. 3. The local protein mobility as analyzed by the B-factors, indicating the relative vibrational motion of different regions of the structure are shown for HPA (a), HPA-ascorbic acid complex (b), and HPA-folic acid complex (c). Here, low B-factors (blue) indicates a well-ordered structure, whereas, a large B-factors (red) indicates a conformational disorder. Order to disorder was represented as darker-blue < lighter-blue < green < yellow < orange < red. The complementary time averaged root mean square fluctuation (RMSF) values of the Cα atoms in individual residues of the polypeptide chain in the three structures (d), namely, HPA (black), HPA-ascorbic acid complex (blue), and, HPA-folic acid complex (red).

Fig. 4. Polypeptide chain representation of β-strands and α-helices of HPA-ascorbic acid complex (a), and HPA-folic acid complex (b). The inhibitors are highlighted in yellow. Hydrogen bonds are depicted as black dashed lines. The active site residues are highlighted in

green. The β-strands and helices represented in red denote the chains that interact with ascorbic/folic acid and are proposed to being involved in the conformational scrambling of HPA catalytic functions. The β-sheets in blue represent the TIM barrel. Black spheres represent ions (Ca and Cl).

Table legends

Table 1. Kinetics of inhibition of HPA by ascorbic acid and folic acid.

Inhibitor	K_m^{app} (mg mL^{-1})					V_{max}^{app} (mM maltose min^{-1})					K_{ic} (mg mL^{-1})	K_{in} (mg mL^{-1})	$\frac{1}{K_{ic}}$ (mg mL^{-1})
	a	b	c	d	e	a'	b'	c'	d'	e'			
Ascorbic acid	3.36±0.31	4.67±0.61	3.92±0.62	3.52±0.56	3.73±0.85	3.58±0.10	3.54±0.17	2.80±0.15	2.10±0.10	1.60±0.12	1.75±0.32	2.20±0.36	0.57±0.08
Folic acid	2.10±0.58	2.78±0.76	2.91±1.13	3.91±1.47	11.46±5.22	3.23±0.08	2.99±0.09	2.94±0.56	2.85±0.59	3.02±0.37	2.30±0.08	_	0.43±0.01

Data are treatment of means (n = 3). P > 0.05 for all non-linear fits indicating residuals are not clustered or heteroscedastic. Concentration of ascorbic acid for the study were 0, 0.325, 0.65, 1.25, and 2.5 mg mL^{-1}, and, for folic acid were 0, 2.5, 5, 10, 20 mg mL^{-1}.

Parameters indicate; the inhibitor dissociation constants, K_{ic} for competitive inhibition and K_{in} for non-competitive inhibition. $\frac{1}{K_{ic}}$ denotes inhibitor association constant.

Table 2. Quenching parameters calculated from the interaction of ascorbic acid and folic acid with HPA.

Inhibitor	T	k_q	K_A		K_{FQ}	n	ΔH°	ΔG°	ΔS°	Redshift λ_{em}^{max}
	(K)	(× 10^4 L mol.s^{-1})	(× 10^4 L mol^{-1})	(× 10^{-2} mg mL^{-1})	(× 10^4 L mol^{-1})		(kJ mol^{-1})	(kJ mol^{-1})	(J $mol^{-1}.K^{-1}$)	(nm)
Ascorbic acid	300	0.32	1.37	1.28	0.76	2.33	-0.40	-10.86	34.85	_
	310	0.38	1.36	1.29	0.86	1.90	_	-11.21	36.16	_
Folic acid	300	2.16	5.79	0.76	4.03	1.51	-2.16	-12.16	33.31	5
	310	2.38	5.63	0.78	4.15	1.69	_	-12.49	40.30	6

Data are treatments of means (n = 2). Parameters indicate; T as temperature, k_q as bimolecular quenching constant, K_A as binding constant, K_{FQ} as apparent static quenching constant, n as binding sites, ΔH^o as *enthalpy change,* ΔS^o as entropy change, and ΔG^o as free energy change.

15 **Highlights**

16 • Water-soluble vitamins show ability to control starch digestion.

17 • The TIM barrel rails the inhibition of α-amylase activity by ascorbic acid.

18 • α-amylase inhibition by folic acid is aided via loop 3, 7 conformational ordering.

19 • Complementary experimental and computational analyzes are discussed.

20

21

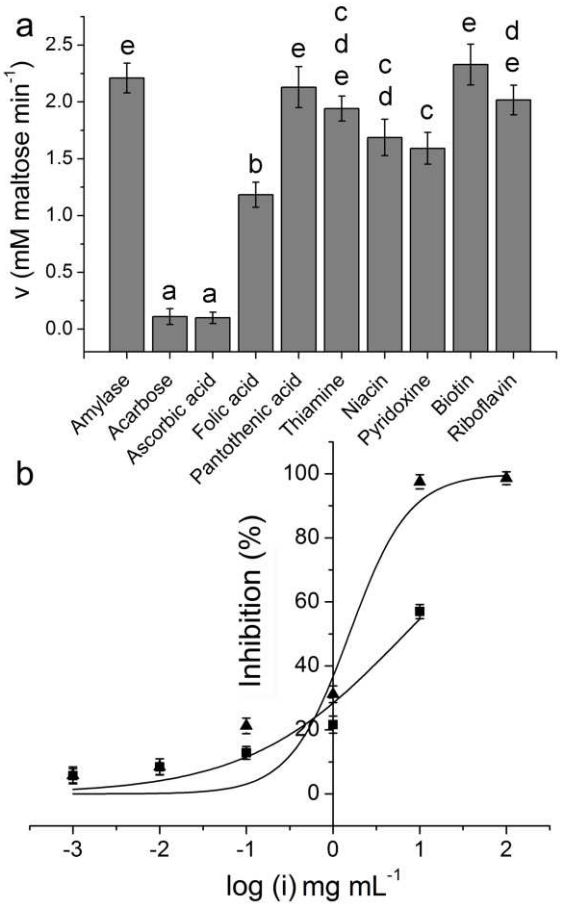

22

23

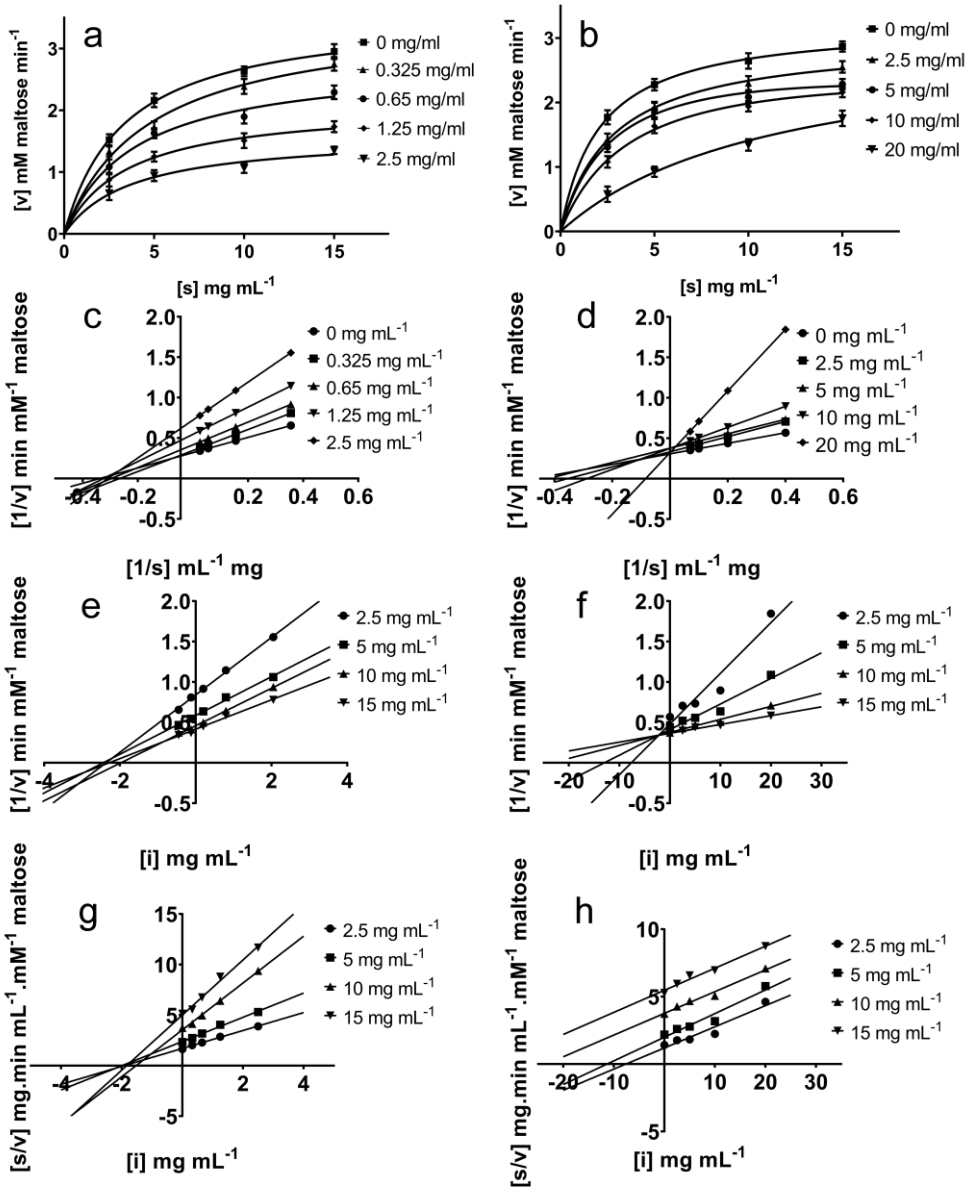

24

25

40

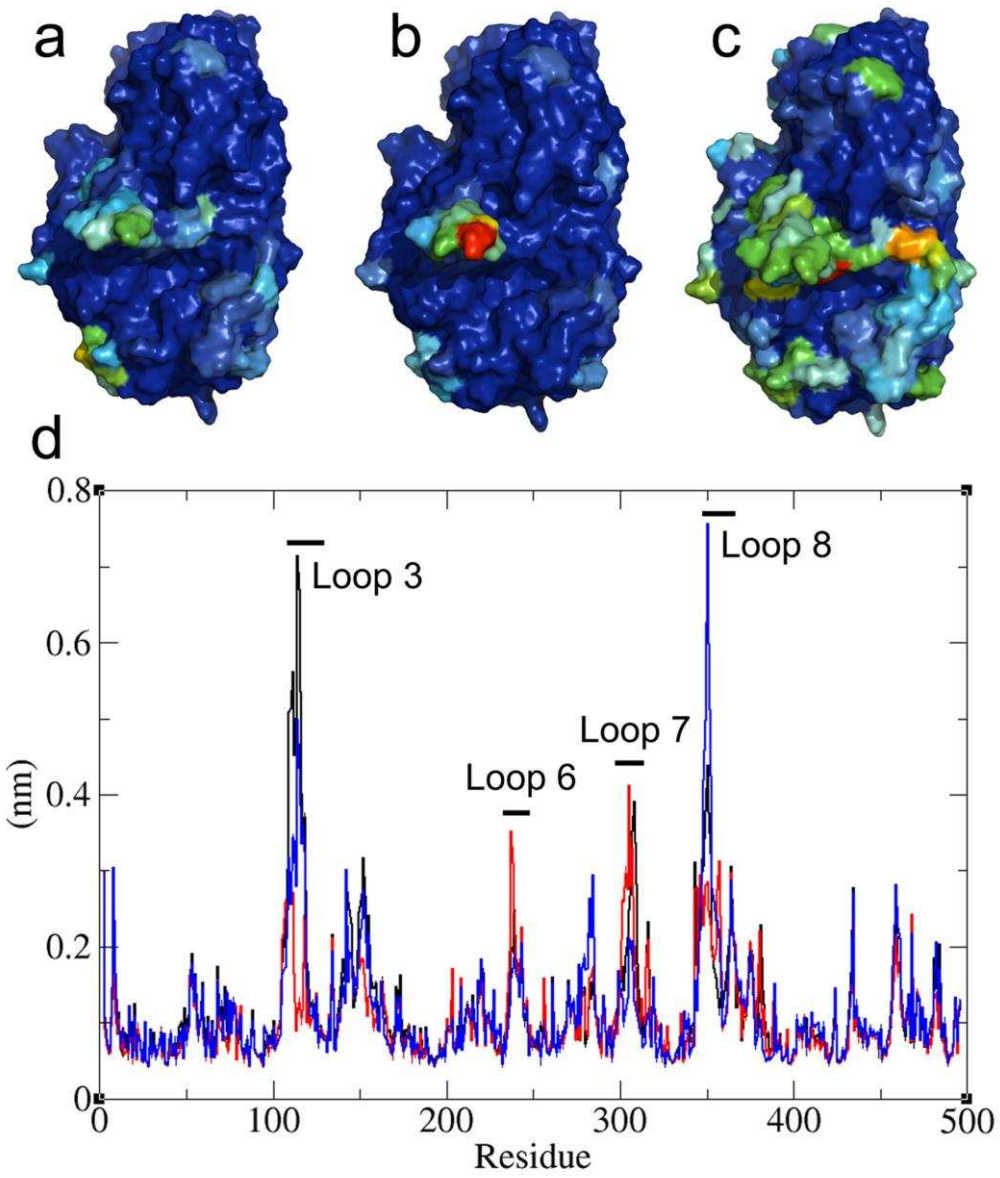

26

27

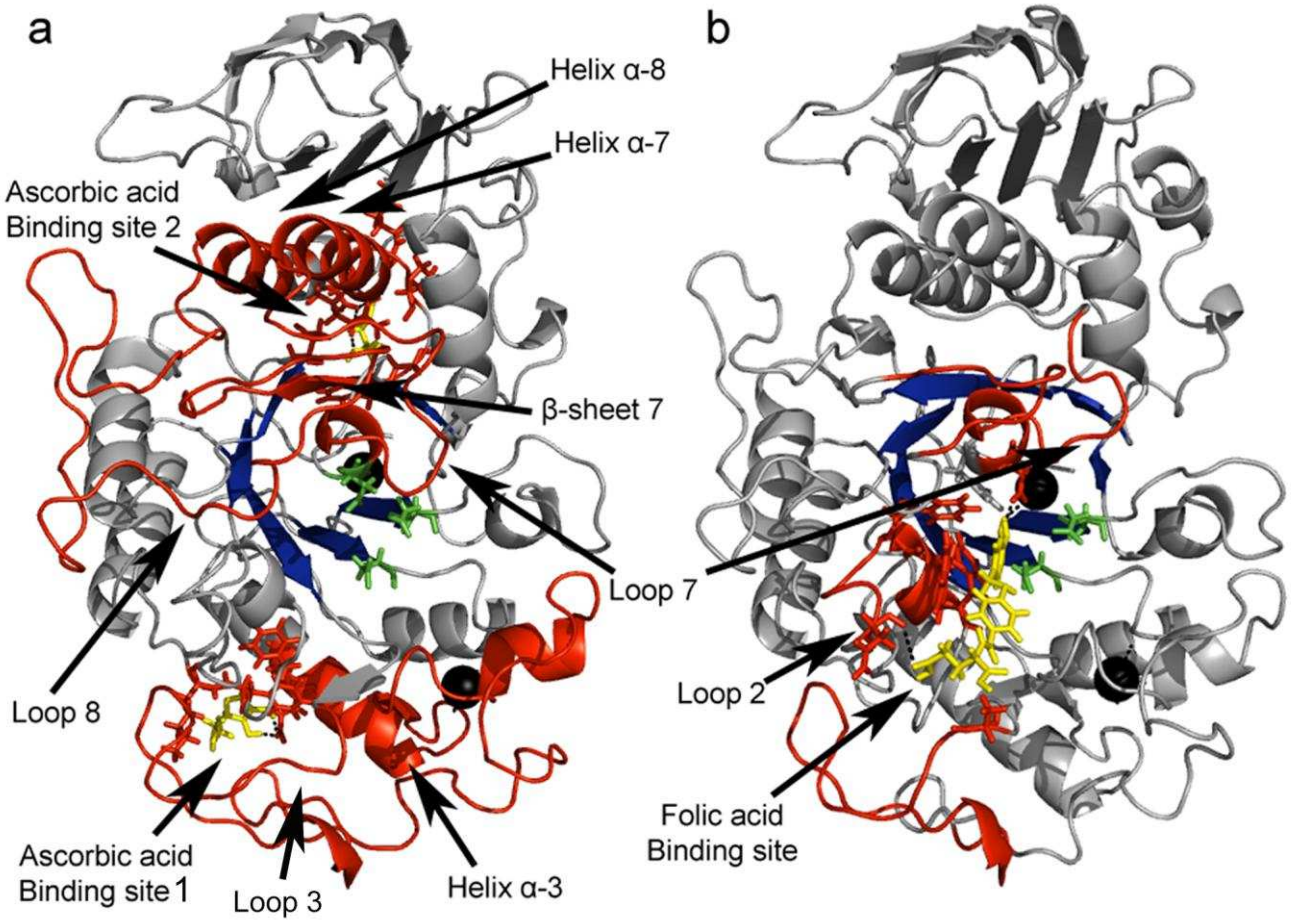

28